

Development of pulsed laser-assisted thermal relaxation technique for thermal characterization of microscale wires

Jiaqi Guo,¹ Xinwei Wang,^{2,a)} David B. Geohegan,³ Gyula Eres,³ and Cécile Vincent⁴

¹*Department of Mechanical Engineering, N104 Walter Scott Engineering Center, The University of Nebraska-Lincoln, Lincoln, Nebraska 68588-0656, USA*

²*Department of Mechanical Engineering, 3027 H.M. Black Engineering Building, Iowa State University, Ames, Iowa 50011-2161, USA*

³*Materials Science and Technology Division and Center for Nanophase Materials Sciences, Oak Ridge National Laboratory, 1 Bethel Valley Road, MS-6056, Oak Ridge, Tennessee 37831-6056, USA*

⁴*ICMCB, CNRS, University of Bordeaux I, 87 Avenue A. Schweitzer, 33600 Pessac, France*

(Received 1 December 2007; accepted 25 March 2008; published online 5 June 2008)

A transient technique is developed to measure the thermal diffusivity of one-dimensional microscale wires. In this technique, the thin wire is suspended over two copper electrodes. Upon fast (nanosecond) pulsed laser irradiation, the wire's temperature will quickly increase to a high level and then decrease gradually. Such temperature decay can be used to determine the sample's thermal diffusivity. To probe this temperature evolution, a dc is fed through the wire to sensor its voltage variation, from which the thermal diffusivity can be extracted. A 25.4 μm thin Pt wire is characterized to verify this technique. Sound agreement is obtained between the measured data and reference value. Applying this pulsed laser-assisted thermal relaxation technique, the thermal diffusivity of multiwall carbon nanotube bundles and microscale carbon fibers is measured. Detailed analysis is conducted to study the effect of the wire embedded in the paste/base on the final measurement result. © 2008 American Institute of Physics. [DOI: [10.1063/1.2936873](https://doi.org/10.1063/1.2936873)]

I. INTRODUCTION

One-dimensional micro-/nanostructures, such as carbon nanotubes (CNTs) and micro-/nanowires, have attracted growing interests and are expected to find broader applications in different areas such as mechanical strength enhancement, novel chemical and optical sensing, as well as thermal-electrical and chemical-electrical energy conversion. Accordingly, knowledge of thermal transport in these micro-/nanoscale wires/tubes becomes considerably indispensable to their future applications. Several techniques have been developed to characterize the thermophysical properties of micro-/nanoscale wires/tubes, like the 3ω method¹⁻³ and microfabricated device method.^{4,5} Recent studies in our group also focus on the thermophysical properties measurement of individual one-dimensional micro-/nanoscale structures. At present, an optical heating and electrical thermal sensing (OHETS) technique,⁶⁻⁸ a transient electrothermal (TET) technique,^{9,10} and a transient photoelectrothermal (TPET) technique¹¹ have been developed to measure the thermophysical properties of wires/tubes at micro-/nanoscales.

For the OHETS technique, a periodically modulated laser beam is used to irradiate the sample, leading to periodical changes in temperature and electrical resistance of the sample. A small dc current is fed to the sample to probe its periodical resistance variation. From the phase shift difference between the voltage variation and laser beam, the thermal diffusivity of the sample can be determined. This steady state technique has been used to measure the thermophysical properties of metallic and nonconductive one-dimensional

micro-/nanoscale structures.⁶⁻⁸ The OHETS technique requires a relatively long measurement time (usually several hours) and suffers from a low signal level (microvolts), which is also encountered in the 3ω method.¹⁻³ For the two transient techniques—TET and TPET—a step dc current and cw laser beam are used, respectively, to heat the sample wire. Upon heating, it will take a certain time for the wire to reach its steady thermal state. The time taken to reach this steady state (characteristic time)⁹⁻¹¹ is strongly related to the thermophysical properties of the wire and its length. From the temperature evolution, the thermal diffusivity of the sample can be extracted. The TET and TPET techniques feature significant signal/noise ratio (in millivolts) and only take a few seconds to finish. They can also be used to measure the thermal properties of metallic, nonconductive, and semiconductive wires.⁹⁻¹¹ However, limited by the slow rising time [$\sim 2 \mu\text{s}$ for current in TET (Ref. 10) and $\sim 10 \mu\text{s}$ for laser in TPET (Ref. 11)], both techniques become difficult to measure short wires with relatively high thermal conductivity/diffusivity. For such samples, their characteristic time of heat transfer will be short and comparable to the rising time of the electrical current/laser beam, thereby making the experiment difficult to conduct.

In this paper, a pulse laser-assisted thermal relaxation (PLTR) technique is developed to overcome the drawbacks of the TET and TPET techniques while providing comparable fast experiment implementation and high signal/noise ratio. This technique can be applied to metallic, nonconductive, and semiconductive micro- and nanoscale wires. Compared with the TET and TPET techniques, the technique developed in this work can be used to measure short wires with high thermal conductivity/diffusivity. To test this technique,

^{a)}Author to whom correspondence should be addressed. Tel.: (515) 294-2085. FAX: (515) 294-3261. Electronic mail: xwang3@iastate.edu.

thermal diffusivity measurement of platinum (Pt) wire is conducted. By applying this technique, the thermal diffusivities of two types of multiwall carbon nanotube (MWCNT) bundles and microscale carbon fibers are measured. The experimental principles and physical model development are presented in Sec. II. The experimental details and results are discussed in Sec. III.

II. EXPERIMENTAL PRINCIPLES AND PHYSICAL MODEL DEVELOPMENT

A. Experimental principles

In the PLTR technique, the to-be-measured wire is suspended over two copper electrodes. Silver paste is placed at the wire/electrode contacts to enhance the mechanical and electrical connection. When running the experiment, a nanosecond laser pulse is used to irradiate the sample wire uniformly to induce a sudden temperature increase (ΔT). Right after the pulsed heating, the temperature of the wire will gradually go down. Such temperature relaxation is strongly determined by the sample's thermal diffusivity and length. For instance, with the same length, if the wire has a larger thermal diffusivity, it will take a shorter time for the temperature to go down and reach its steady state. From this temperature relaxation history, the thermal diffusivity of the wire can be determined. In order to probe its temperature evolution, a small dc is fed through the wire for the reason that the temperature change will correspondingly lead to a resistance change. As a result, there will be a resistance change (ΔV) over the wire. When the temperature change is not large, it is physically reasonable to assume that the resistance change of the wire has a linear relationship with its average temperature change. Therefore, the measured $\Delta V \sim t$ (t , time) shares the same shape as the $\Delta T \sim t$ curve. The shape of the normalized $\Delta V \sim t$ curve can be used to determine the thermal diffusivity of the sample.

B. Physical model development

Although in the experiment the laser only heats one side of the sample, the heat transfer will happen quickly from the heated side to other regions of the sample to make the temperature uniform over its cross section. The time (t_1) taken to reach this uniform temperature distribution over the cross section is much smaller than the characteristic heat transfer time (t_c) along the axial direction. Their ratio is $t_1/t_c \approx (D/L)^2$, where D and L are the diameter and length of the wire, respectively. In our experiment, the length of the wire is significantly greater than its diameter, which will simplify the physical mode to one dimension (in the axial direction of the wire).

For one-dimensional (1D) heat transfer along the wire, the governing equation at time $t \geq 0$ is

$$\frac{\partial(\rho c_p T)}{\partial t} = k \frac{\partial^2 T}{\partial x^2} + \dot{q}, \quad (1)$$

where \dot{q} is the rate of thermal energy generation. $\dot{q} = \dot{q}_1 + \dot{q}_2$, where \dot{q}_1 is the dc heating and \dot{q}_2 is the laser pulse heating. ρ ,

c_p , and k are the density, specific heat, and thermal conductivity of the wire, respectively. In Eq. (1), x indicates the axial direction of the wire. For 1D heat transfer along the wire, the initial condition of the problem is $T(x, t=0) = T_0$, where T_0 is the room temperature. Since the wire dimensions are much smaller than those of the copper electrodes used in the experiments, the temperature at the wire/electrode contacts can be assumed constant because the electrodes are excellent heat sinks. As a result, the boundary conditions at the two ends are described as $T(x=0, t) = T(x=L, t) = T_0$, where L is the wire length. The solution to Eq. (1) can be described as $T(x, t) = T_1(x) + T_2(x, t)$, where $T_1(x)$ is the steady temperature induced by the dc, and $T_2(x, t)$ by the pulsed laser heating. Since we are only interested in the temperature evolution caused by the pulsed laser heating, its governing equation can be described as

$$\frac{\partial(\rho c_p T_2)}{\partial t} = k \frac{\partial^2 T_2}{\partial x^2} + \dot{q}_2, \quad (2)$$

with homogeneous boundary conditions and initial conditions, $T_2(x=0, t) = T_2(x=L, t) = 0$ and $T_2(x, t=0) = 0$. Here, T_2 only represents the temperature variation induced by the pulsed laser heating. The pulsed laser heating source can be simplified as

$$\dot{q}_2 = \begin{cases} s, & 0 \leq t \leq \Delta t \\ 0, & t > \Delta t. \end{cases} \quad (3)$$

Here, Δt is the laser pulse width, and we assume the laser intensity is constant during Δt . Since the laser heating time ($\sim 10^{-9}$ s) is significantly smaller than the characteristic time of heat transfer in the sample, the above assumption will have negligible effect on the accuracy of the solution. To make the solution development more feasible, we assume that ρ , c_p , and k are constant and independent of temperature. The solution to the partial differential equation described by Eq. (2) can be obtained by the integral of Green's function,¹²

$$G_{X11}(x, t|x', \tau) = \frac{2}{L} \sum_{m=1}^{\infty} \exp[-m^2 \pi^2 \alpha (t - \tau)/L^2] \times \sin\left(m\pi \frac{x}{L}\right) \sin\left(m\pi \frac{x'}{L}\right). \quad (4)$$

The average temperature of the wire $T_2(t)$ for $0 < t \leq \Delta t$ can be obtained by integration over the wire as

$$T_2(t) = \frac{1}{L} \int_{x=0}^L T_2(x, t) dx = \frac{8sL^2}{k\pi^4} \sum_{m=1}^{\infty} \frac{1 - \exp[-(2m-1)^2 \pi^2 \alpha t/L^2]}{(2m-1)^4}. \quad (5)$$

For time t larger than Δt , we have

$$T_2(t) = \frac{8sL^2}{k\pi^4} \sum_{m=1}^{\infty} \frac{\exp[-(2m-1)^2\pi^2\alpha t/L^2]\{\exp[(2m-1)^2\pi^2\alpha\Delta t/L^2]-1\}}{(2m-1)^4}. \quad (6)$$

Since we are only interested in the relative temperature decay after laser heating, $T_2(t)$ will be normalized as $T_2^* = [T_2(t) - T_{2,\min}]/(T_{2,\max} - T_{2,\min})$. Here, $T_{2,\min}$ is 0 and $T_{2,\max}$ is the maximum temperature rise of the sample. Since the laser heating happens within a very short time, heat transfer in the sample's axial direction during heating can be neglected. Consequently, $T_{2,\max}$ can be calculated as $s\Delta t/\rho c_p$ based on energy conservation. Then, the normalized temperature relaxation can be written as

$$T_2^* = \frac{8L^2}{\alpha\Delta t\pi^4} \sum_{m=1}^{\infty} \frac{\exp[-(2m-1)^2\pi^2\alpha t/L^2]\{\exp[(2m-1)^2\pi^2\alpha\Delta t/L^2]-1\}}{(2m-1)^4}. \quad (7)$$

Since the pulse width Δt in our experiment is only 7 ns, $\exp[(2m-1)^2\pi^2\alpha\Delta t/L^2]$ can be simplified as $1 + (2m-1)^2\pi^2\alpha\Delta t/L^2$ using Taylor expansions. People may think that even if Δt is very small, the term of $(2m-1)^2$ will increase and lead to the inaccurate estimation in Taylor expansions. To justify our approximation, further convergence study is carried out. To make the summation converge, the value of the term related to m should be less than 10^{-3} of the summation from terms 1 to $m-1$. We found that the maximum term used to converge is $m=15$, which means that the exponent $(2m-1)^2\pi^2\alpha\Delta t/L^2$ is small enough, and our approximation still applies. So, Eq. (7) can be simplified as

$$T_2^* = \frac{8}{\pi^2} \sum_{m=1}^{\infty} \frac{\exp[-(2m-1)^2\pi^2\alpha t/L^2]}{(2m-1)^2}. \quad (8)$$

Equation (8) shows that for any kind of material of arbitrary length, the normalized temperature relaxation follows the same shape with respect to the Fourier number $\text{Fo} (= \alpha t/L^2)$. In the above thermal analysis, laser heating over the sample is assumed uniform. In practice, the laser beam has a Gaussian distribution in space. To suppress the effect of the nonuniformity of the laser beam, a relatively large laser beam spot is used (around 1 cm in diameter), which is much larger than the sample length. This ensures that the laser intensity distribution over the sample will be very uniform.

C. Methods to determine the thermal diffusivity

Figure 1 shows a typical normalized temperature relaxation curve as an example to discuss the two data analysis methods for determining the sample's thermal diffusivity. The first method is based on a characteristic point on the temperature relaxation curve. It is seen from Eq. (8) that the normalized temperature is only a function of the Fourier number $\text{Fo} = \alpha t/L^2$. Therefore, one single point on the $T_2^* \sim t$ curve can be used to determine the thermal diffusivity of the wire directly. The best characteristic point should have the property that both the y axis (normalized temperature) and x axis (time) have very high sensitivity to a small change of $\delta\alpha$. That is to say, we need the product $\delta T_2^* \delta t$ to have the maximum value when the thermal diffusivity changes by $\delta\alpha$, where $\delta T_2^* = \partial T_2^*/\partial\alpha \cdot \delta\alpha$ and $\delta t = \partial t/\partial\alpha \cdot \delta\alpha$. In order to get

the maximum sensitivity, the term $\partial T_2^*/\partial\alpha \cdot \partial t/\partial\alpha$ should reach its maximum value. It is not difficult to find that $\partial T_2^*/\partial\alpha \cdot \partial t/\partial\alpha = \partial T_2^*/\partial\text{Fo} \cdot L^2 \cdot \text{Fo}^2/\alpha^3$.

Using numerical methods and Eq. (8), we find that the best characteristic point corresponds to the normalized temperature T_2^* of 0.1097. The corresponding Fourier number is 0.2026, as shown in Fig. 1. When using the characteristic point method, once the characteristic time (t_c) is identified from the $T_2^* \sim t$ curve when the normalized temperature goes down to 0.1097, the thermal diffusivity of the sample can be calculated as $\alpha = 0.2026L^2/t_c$. In order to better determine the characteristic point from obtained experimental data, a small set of data points around the characteristic point is used with linear fitting to determine the characteristic point.

The second method to determine the thermal diffusivity of the sample is based on global data fitting of the temperature relaxation curve. In this method, the normalized temperature decrease is calculated using Eq. (8) by using different trial values of thermal diffusivity. The trial value giving the best fit (least squares) of the experimental data is taken as the sample's thermal diffusivity.

III. EXPERIMENTAL DETAILS AND RESULTS

A. Experimental setup and calibration

In the experiment, a current source (Keithley 6221) is used to provide a constant dc through the sample. A neodymium-doped yttrium aluminum garnet laser operated at periodical pulse mode is used to heat the sample. The pulse width of the laser (7 ns) is much shorter than the char-

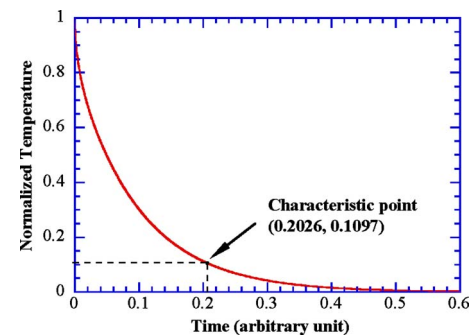


FIG. 1. (Color online) Normalized theoretical curve to show the data analysis methods.

TABLE I. Details of experimental conditions for the Pt wire.

	Data 1	Data 2
Length (mm)	3.513	
Diameter (μm)	25.4	
Resistance at room temperature (Ω)	0.791	
dc (mA)	30	
Voltage across the wire after feeding the current (mV)	29.12	29.01
Voltage increase caused by laser pulse heating (mV)	1.795	1.026
Thermal diffusivity by characteristic point ($10^{-5} \text{ m}^2 \text{ s}^{-1}$)	2.47	2.56
Thermal diffusivity by least squares fitting ($10^{-5} \text{ m}^2 \text{ s}^{-1}$)	2.53	2.50

acteristic time t_c for the measured samples. A high speed digital oscilloscope TDS7054 with a proper offset is used to capture the fine change of the voltage over the sample. In order to minimize the influence of air convection, the wire is housed in a vacuum at 1×10^{-3} Torr.

To verify the PLTR technique and the theoretical model developed in this work, a $25.4 \mu\text{m}$ thick Pt wire is measured first. The Pt wire of 3.513 mm length is placed over two copper electrodes, and silver paste is applied on the wire/copper contacts to enhance the thermal and electrical connection. During the experiments, two different pulse energies are used to heat the sample and record the experimental data at the same dc of 30 mA. The experimental conditions are all listed in Table I. Both data analysis methods are used to determine the thermal diffusivity. By using the least squares fitting method, the thermal diffusivities based on the two sets of data are fitted to be 2.53×10^{-5} and $2.50 \times 10^{-5} \text{ m}^2 \text{ s}^{-1}$, respectively, close to the literature value of $2.51 \times 10^{-5} \text{ m}^2 \text{ s}^{-1}$ (at 300 K).¹³ The characteristic point method also gives close thermal diffusivities of 2.47×10^{-5} and $2.56 \times 10^{-5} \text{ m}^2 \text{ s}^{-1}$, respectively. Figure 2 shows the fitting results for data 1 using both data analysis methods. Sound agreement is observed between the fitting results and the experimental data for global data fitting.

To further understand the experiment, we take data 1 of the Pt wire as an example to estimate the temperature rise after pulsed laser heating. Based on the measured voltage rise ΔV over the sample, the average temperature increase can be estimated using the equation $\Delta V/V \approx \varepsilon \Delta T$, where ε is the temperature coefficient of resistance for Pt and V is the voltage across the Pt wire when feeding the current I (before laser heating). In the experiment, ΔV is 1.795 mV and V is 29.12 mV. Taking ε as $3.927 \times 10^{-3} \text{ K}^{-1}$,¹⁴ the overall average temperature increase is calculated to be $15.7 \text{ }^\circ\text{C}$. In order to have sound signals in the PLTR technique, a temperature increase of tens of degrees is required. For this level of temperature increase, the R - T relation for most metals can be treated linear with sound accuracy. For example, Pt has a constant temperature coefficient of resistance ($3.927 \times 10^{-3} \text{ K}^{-1}$) within the temperature range of 0 – $100 \text{ }^\circ\text{C}$.¹⁴ The nonlinear feature in the R - T relation will induce some second-order negligible uncertainty in final data processing.

In Sec. II B, when deriving Eq. (2) from Eq. (1), we assume weak coupling between T_1 and T_2 . One obvious issue is that when the laser pulse increases the wire temperature, the wire resistance will change (ΔR). This will lead to a

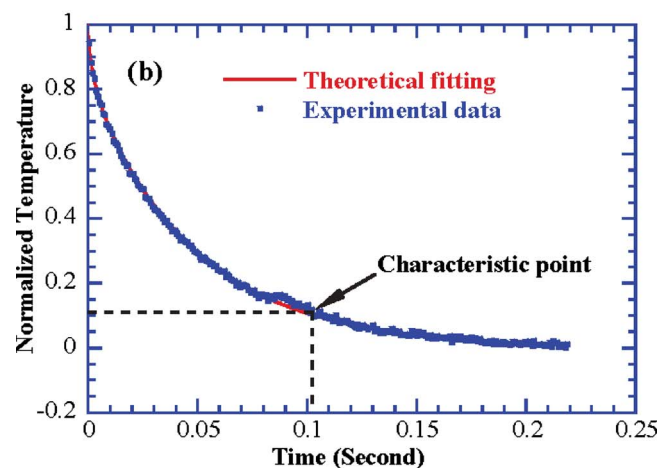
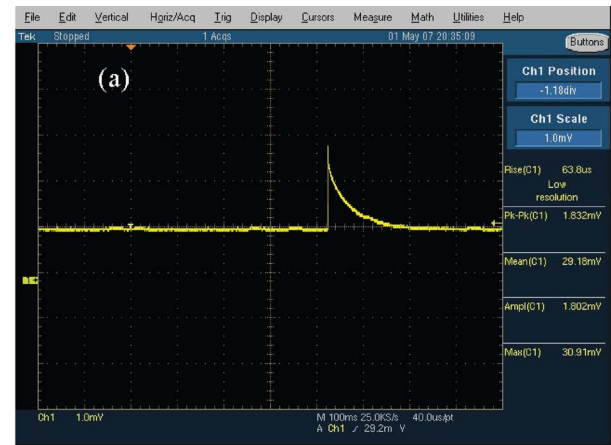


FIG. 2. (Color online) (a) Captured picture from the oscilloscope showing the voltage variation over the Pt wire for experimental data 1 and (b) the normalized temperature vs the theoretical fitting using both data analysis methods.

small change in \dot{q}_1 (dc heating). Such small change in heating will give rise to another temperature and resistance change (ΔR_2) of the wire. In the experiment, the measured voltage change, in fact, includes the effect of ΔR_2 . On the other hand, ΔR_2 is much smaller than ΔR . Taking the Pt wire experiment (data 1) as an example, the maximum resistance change by the laser pulse is around 0.049Ω . Therefore, the total electrical heating in the wire changes by about $4.41 \times 10^{-5} \text{ W}$. Such heating will increase the average temperature of the wire by $0.36 \text{ }^\circ\text{C}$. This temperature increase is much smaller compared with the overall temperature rise of the wire ($15.7 \text{ }^\circ\text{C}$). Therefore, it is conclusive that the heating change induced by the small electrical current through the wire can be neglected in the experiment.

B. Measurement of MWCNT bundles

In this section, two types of MWCNT bundles, fabricated at the Oak Bridge National Laboratory, are measured by using the established thermal relaxation technique. Scanning electron microscopy (SEM) study of the samples shows that there are MWCNTs with diameters from 30 to 50 nm inside the bundle. The alignment of the MWCNTs does not

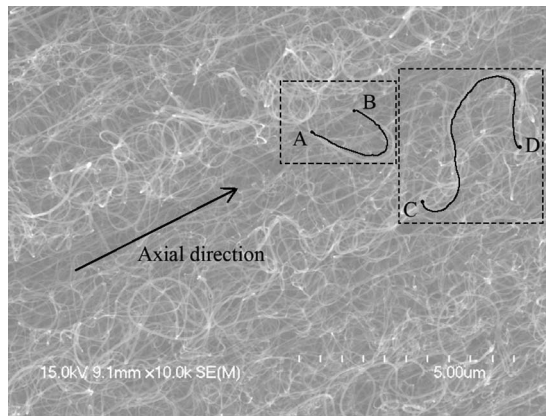


FIG. 3. SEM picture showing the thread alignment inside one type 2 MWCNT bundle.

follow the axial direction of the bundle, as shown in Fig. 3 (type 2 MWCNT). The typical diameters of the MWCNT bundles are 200 and 30 μm for type 1 and type 2, respectively. Since the diameter of the type 1 MWCNT bundle is too thick, it will take a relatively long time to make the temperature uniform on the cross section of the bundle after pulsed laser heating of one side of the bundle. As a result, the heat transfer will become two dimensional. To measure the type 1 MWCNT bundle, a thinner bundle ($\sim 20 \mu\text{m}$) is peeled off it to conduct the measurement.

In the experiment, the MWCNT bundles are connected between two copper electrodes using silver paste, as shown in Fig. 4. Table II shows the length, resistance, and other parameters of the MWCNT bundles measured in the experiment. When conducting experiments, it is observed that the temperature coefficient of resistance for the MWCNT bundles is negative, just like graphite fibers. The characteristic point and least squares fitting methods are used to determine the thermal diffusivity of the samples. For the first type of bundle, the thermal diffusivity is fitted to be 1.09×10^{-5} and $1.05 \times 10^{-5} \text{ m}^2 \text{ s}^{-1}$ using the characteristic point and least squares fitting methods, respectively. For the second type of bundle, the fitted thermal diffusivities are 1.42×10^{-5} and $1.50 \times 10^{-5} \text{ m}^2 \text{ s}^{-1}$ by using the two methods. Figure 5 shows the characteristic point and least squares fitting methods for both types of MWCNT bundles. The sample is measured several times to check the repeatability of the technique. A measurement uncertainty of about 6.5% is observed. In order to check the reliability of measured thermal diffusivity for the two types of MWCNT bundles, the TET technique is used to measure the thermal diffusivity as well. For the type 1 MWCNT bundle, the TET measurement is conducted at the same time of PLTR technique and the measured average thermal diffusivity is $1.05 \times 10^{-5} \text{ m}^2 \text{ s}^{-1}$, which further verifies the reliability of PLTR technique and the thermal diffusivity obtained from PLTR technique. The average thermal diffusivity measured using the TET technique for the type 2 MWCNT bundle is $1.18 \times 10^{-5} \text{ m}^2 \text{ s}^{-1}$, which is conducted one day after PLTR measurement and is slightly smaller than the value obtained from PLTR technique. This is probably due to the extra vacuum pumping leading to slightly structure change, like CNT

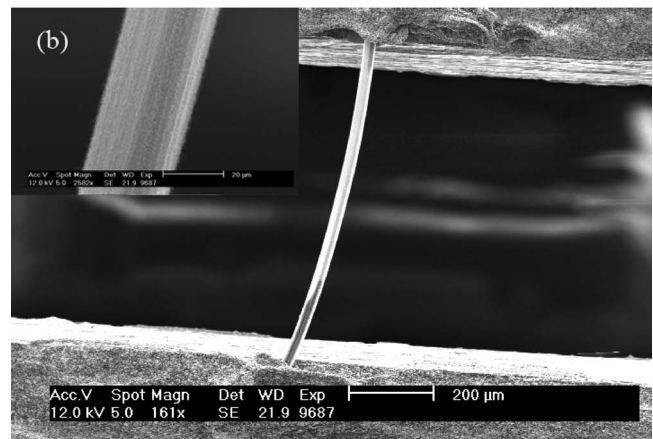
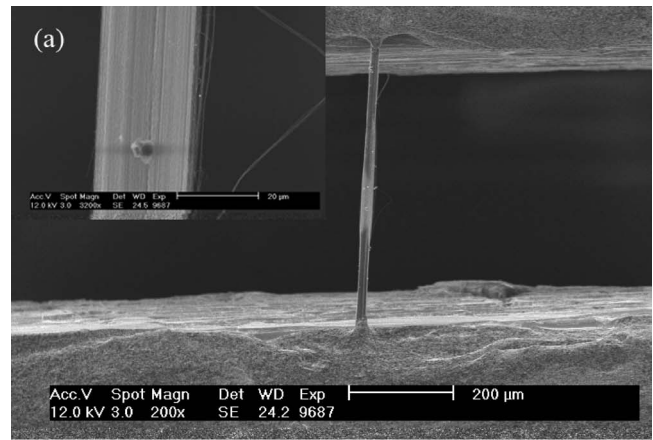


FIG. 4. SEM pictures of the two types of MWCNT bundles [(a) for type 1 and (b) for type 2] measured in the experiment.

breaking inside. Furthermore, the TET technique is employed again to measure the intact (unpeeled) type 1 MWCNT bundle with a diameter around 200 μm . The measured thermal diffusivity is $2.78 \times 10^{-5} \text{ m}^2 \text{ s}^{-1}$, which is more than two times the thermal diffusivity of the peeled bundle. Through this measurement, we can see that the peeling process can ruin the inside structure of bundle.

The random alignment of the CNTs in the bundle has a significant contribution to the measured low thermal diffusivity. Based on the alignment shown in Fig. 3, some first-order estimation can be conducted to evaluate the real thermal diffusivity of single MWCNTs. Two typical MWCNTs are picked and analyzed. One is between points A and B, as

TABLE II. Details of experimental conditions and results for MWCNT bundles.

	Type 1	Type 2
Length (μm)	566.4	800.9
Diameter (μm)	23.3	29.7
dc (mA)	0.2	0.1
Voltage across the wire after feeding the current (mV)	53.3	57.2
Voltage increase caused by laser pulse heating (mV)	-0.96	-1.07
Thermal diffusivity by characteristic point ($10^{-5} \text{ m}^2 \text{ s}^{-1}$)	1.09	1.42
Thermal diffusivity by least squares fitting ($10^{-5} \text{ m}^2 \text{ s}^{-1}$)	1.05	1.50

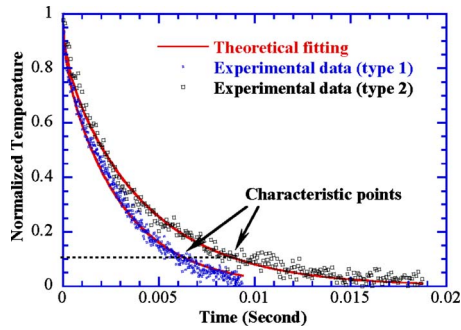


FIG. 5. (Color online) The normalized temperature vs the theoretical fitting for two types of MWCNT bundles.

shown in Fig. 3. The length between A and B is $1.125 \mu\text{m}$ in the axial direction. However, the real length of the MWCNT from A to B is $3.542 \mu\text{m}$, shown by the black curve in the figure. As the thermal diffusivity (α) is proportional to the square of length (L^2) in data processing, the thermal diffusivity of this single MWCNT is estimated to be $1.45 \times 10^{-4} \text{ m}^2 \text{ s}^{-1}$, which is about ten times the thermal diffusivity of the MWCNT bundle ($1.46 \times 10^{-5} \text{ m}^2 \text{ s}^{-1}$ for type 2). Similarly, taking the MWCNT between C and D for analysis, the direct length between C and D is $2.583 \mu\text{m}$, while the MWCNT measures about $6.389 \mu\text{m}$ from C to D. The thermal diffusivity of this single MWCNT is estimated to be $8.93 \times 10^{-5} \text{ m}^2 \text{ s}^{-1}$. For more curved CNTs (so many as shown in Fig. 3), their thermal diffusivities will be much larger than $8.93 \times 10^{-5} \text{ m}^2 \text{ s}^{-1}$. Our estimation concludes that the real thermal diffusivity of MWCNTs should be about ten times the measured value. If considering the effect of the thermal contact resistance between CNTs, the real thermal diffusivity of single MWCNTs can be even higher.

C. Measurement of individual microscale carbon fibers

In this section, individual microscale carbon fibers (K223HG) from the Mitsubishi Chemical U.S.A., Inc. are measured using the PLTR technique. The sample used in the experiment has a resistance of $15.2 \text{ k}\Omega$ and a length of about $342 \mu\text{m}$. The SEM picture of the carbon fiber is shown in Fig. 6. Table III shows all the detailed experiment

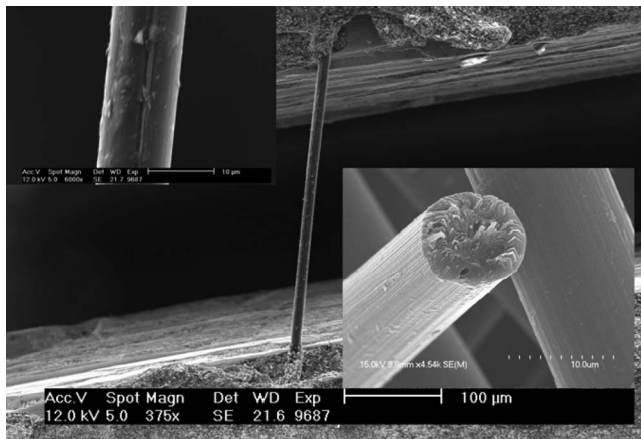


FIG. 6. SEM pictures of the characterized carbon fiber.

TABLE III. Details of experimental conditions and results for the carbon fiber.

	Data 1	Data 2
Length (μm)	342.0	
Diameter (μm)	11.3	
Resistance of sample ($\text{k}\Omega$)	15.2	
dc (mA)	5	7
Voltage across the wire after feeding the current (mV)	60.3	84.1
Voltage increase caused by laser pulse heating (mV)	-1.06	-1.95
Thermal diffusivity by characteristic point ($10^{-5} \text{ m}^2 \text{ s}^{-1}$)	9.96	10.3
Thermal diffusivity by least squares fitting ($10^{-5} \text{ m}^2 \text{ s}^{-1}$)	9.55	9.85

parameters and results. Both the characteristic point and global data fitting methods are applied to determine the thermal diffusivity of the carbon fiber. The thermal diffusivities are determined as 9.96×10^{-5} and $9.55 \times 10^{-5} \text{ m}^2 \text{ s}^{-1}$ for data 1 and 1.03×10^{-4} and $9.85 \times 10^{-5} \text{ m}^2 \text{ s}^{-1}$ for data 2. Figure 7 shows the fitting curve for data 2 using the least squares data fitting and characteristic point methods. Experiments are conducted for a number of rounds and the repeatability is found to be better than 5.2%. If the density ($2.21 \times 10^3 \text{ kg m}^{-3}$) and specific heat ($7.09 \times 10^2 \text{ J kg}^{-1} \text{ K}^{-1}$) of graphite at 300 K (Ref. 13) are taken for the carbon fiber, its thermal conductivity is calculated to be $155 \text{ W m}^{-1} \text{ K}^{-1}$ based on the average value of the measured thermal diffusivity.

D. Uncertainty analysis

When running the experiment, silver paste is applied to enhance the contact between the wire and copper electrodes. However, silver paste, generally speaking, has a very low thermal conductivity compared with copper. The thermal energy cannot be quickly conducted away from the wire to the electrodes. In addition, if the wire has a thermal conductivity much higher than that of the electrodes/paste, heat transfer will preferentially happen along the wire embedded in the silver paste (as shown in Fig. 8). This means that the temperature at the wire/electrode contact might not be actually fixed to the room temperature, especially for wires with high thermal conductivity. This effect could have appreciable effect on the measurement results and has not been studied well in the past. In order to precisely investigate the heat transfer at the contact point and the accuracy of the assump-

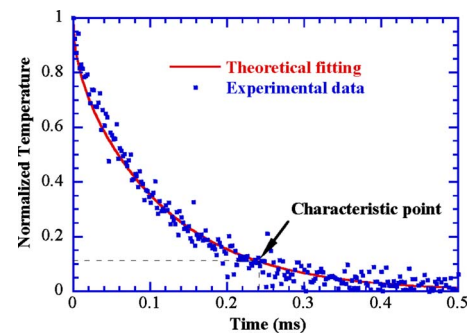


FIG. 7. (Color online) The normalized temperature vs the theoretical fitting for the carbon fiber (data 2).

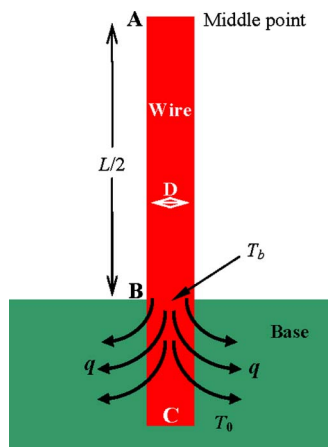


FIG. 8. (Color online) The schematic to show the heat transfer along the wire embedded in the base/paste.

tion (wire/electrode contact is at the room temperature) used in our solution development, numerical simulation is used to study the heat transfer along the wire and from the embedded wire to the electrode base.

In the simulation, the finite difference method is used in the two-dimensional (2D) model (radial and axial directions). The thermal properties of the base ($k=202.5 \text{ W m}^{-1} \text{ K}^{-1}$ and $\rho c_p=1.97 \times 10^6 \text{ J m}^{-3} \text{ K}^{-1}$) are taken as the average values of the copper ($k=401 \text{ W m}^{-1} \text{ K}^{-1}$ and $\rho c_p=3.44 \times 10^6 \text{ J m}^{-3} \text{ K}^{-1}$)¹³ and silver paste ($k=4 \text{ W m}^{-1} \text{ K}^{-1}$ and $\rho c_p=5.01 \times 10^5 \text{ J m}^{-3} \text{ K}^{-1}$).^{15,16} Since the measured carbon fiber has relatively high thermal conductivity, this analysis is conducted for a carbon fiber, which has the close dimension as the measured one: length of $300 \mu\text{m}$, diameter of $10 \mu\text{m}$, and ρc_p of $1.5336 \times 10^6 \text{ J m}^{-3} \text{ K}^{-1}$. Carbon fibers with different thermal conductivities from 10 to $500 \text{ W m}^{-1} \text{ K}^{-1}$ are studied using the numerical simulation to obtain the idea about how much the heat transfer through the embedded fiber affects the final measurement results. The mesh sizes used in the simulation are $\Delta x=1 \mu\text{m}$ and $\Delta r=1 \mu\text{m}$. The explicit method is utilized to calculate the heat transfer in the fiber and electrodes with a time step varying from 10^{-10} to 10^{-7} s, depending on the sample's thermal conductivity. An extreme case (with base thermal conductivity of $1 \text{ W m}^{-1} \text{ K}^{-1}$ and carbon fiber thermal conductivity of $500 \text{ W m}^{-1} \text{ K}^{-1}$) is calculated first to explore the temperature distribution inside the base region and, meanwhile, to verify the numerical program. Figure 9 shows the 2D temperature rise distribution at the time of 0.3 ms. From this case, we can see that the temperature at the wire/base contact is far above zero, which means that the heat transfer model in

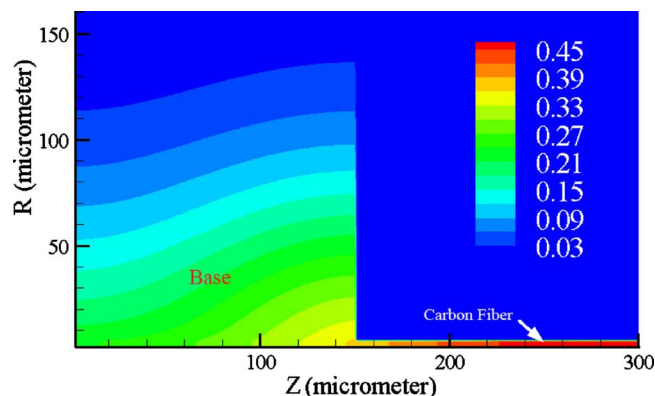


FIG. 9. (Color online) 2D temperature distribution at 0.3 ms for the extreme case ($k_b=1 \text{ W m}^{-1} \text{ K}^{-1}$, $k_w=500 \text{ W m}^{-1} \text{ K}^{-1}$, and $\rho c_p=1.5336 \times 10^6 \text{ J m}^{-3} \text{ K}^{-1}$).

the PLRT technique cannot be applied to samples having much higher thermal conductivity than the base.

To study the effect of heat transfer along the wire in the base/paste, virtual experiments are conducted. In this study, numerical calculations are first conducted using the finite difference method to calculate the temperature relaxation of the fiber upon pulsed laser heating. Then, global data fitting of this temperature relaxation is conducted based on the solution Eq. (8) to determine the effective thermal diffusivity/conductivity of the fiber. The fitted thermal conductivity in comparison with the real thermal conductivity of the fiber is summarized in Table IV. From Table IV, we can see that if the thermal conductivity of the fiber is much smaller than the base, the fitted result is close to the real thermal conductivity of the sample. When the thermal conductivity of the sample is larger, the part of the sample embedded in the electrode/paste has more effect on the final fitting result.

To better understand the relationship between the measured thermal conductivity (k_{eff}) and other parameters, such as diameter D , length L , thermal conductivity of the wire (k_w), base (k_b), etc., a first-order estimation can be used based on the steady state thermal resistance analysis even if the experiment here is transient. The thermal resistance from the highest temperature point (middle point of the wire, A) down to the room temperature point (end point of the wire, C) is comprised of two parts, as shown in Fig. 8. One is the conduction thermal resistance of the exposed wire (from point A to B) calculated as $L/(2k_w A)$. The other part is the thermal resistance of the wire embedded in the silver paste (from point B to C). To simplify this theoretical analysis, we assume that the length of the wire embedded in the silver paste is infinite and treat it like a fin. This represents an extreme situation, and the heat transfer rate q_f from this fin can be described as¹⁷

TABLE IV. Numerical simulation results for the effect of the wire embedded in the paste.

Real k (W/m K)	10	20	50	100	200	500
k_{eff} by fitting virtual experimental data	9.81	19.3	47.9	94.3	186	440
Relative error $[(k-k_{\text{eff}})/k]$ (%)	1.9	3.4	4.3	5.7	7.2	12
k_{eff} from Eq. (13)	9.95	19.9	49.4	98.4	195	482
Relative error $[(k-k_{\text{eff}})/k]$ (%)	0.5	0.8	1.2	1.6	2.3	3.6

$$q_f = \sqrt{hPk_w A_c}(T_b - T_0), \quad (9)$$

where h is the equivalent effective convection heat transfer coefficient for the fin, k_w is the thermal conductivity of the fin (wire), P is the fin perimeter, A_c is the cross-sectional area, T_b is the temperature at the contact point, and T_0 is the room temperature. For the sample embedded in the paste, heat transfer happens through conduction. An equivalent effective convection coefficient h_{eff} can be obtained as

$$1/(h_{\text{eff}}\pi Dl) = \ln(D_0/D)/(2\pi l k_b), \quad (10)$$

where D is the diameter of the wire, D_0 ($\sim\sqrt{\alpha_b t_c}$) is a suppositional diameter where the temperature decreases down to the room temperature in the paste, k_b is the thermal conductivity of the base/paste, and l is the length embedded by the silver paste. Taking the first-order estimation of $\ln(D_0/D)$ as 1, we get $h=2k_b/D$. Substituting it into Eq. (9), the thermal resistance [$R_2=q_f/(T_b-T_0)$] of the wire embedded in the paste/base is

$$R_2 \approx \sqrt{2/(k_w k_b \pi^2 D^2)}. \quad (11)$$

In our theoretical development for Eq. (8), we take the second part of the thermal resistance as zero because we assume that the temperature at the two contact points (boundary conditions) is fixed to the room temperature. When taking into account the second part of thermal resistance, the effective thermal conductivity of the wire can be estimated as

$$2L/(k_{\text{eff}}\pi D^2) \approx 2L/(k_w\pi D^2) + \sqrt{2/(k_w k_b \pi^2 D^2)}. \quad (12)$$

The effective thermal conductivity of the sample is

$$k_{\text{eff}} \approx \frac{k_w}{1 + (D/L) \cdot \sqrt{k_w/(2k_b)}}, \quad (13)$$

from which we can see that the effective thermal conductivity is determined by the aspect ratio of the wire and the thermal conductivity ratio k_w/k_b . When the thermal conductivity of the base is very high ($k_w/k_b \ll 1$), the effective thermal conductivity will be very close to the real one of the wire. This is the reason why we try to find highly conductive materials as the electrodes. From Eq. (13), it can be found that if the wire is thin and long (meaning very small D/L), the effective thermal conductivity will become close to the real one. Using Eq. (13), the effective thermal conductivity can be estimated with the knowledge of diameter D , length L , and base thermal conductivity k_w , which are all listed in Table IV. In Table IV, it is observed that although the k_{eff} estimated from Eq. (13) is not exactly the same as that predicted using the finite difference technique, it presents a very close estimation and gives a clear idea about the effect of the base property and wire dimension.

Radiation heat transfer from the wire surface is another important issue for consideration in the PLTR technique. For radiation heat transfer from half of the wire, it can be approximated by $q_{\text{rad}} = \pi\sigma[(T_0 + \Delta T)^4 - T_0^4]DL/2$, where ΔT is the average temperature rise over the sample. Meanwhile, the heat conduction rate is also estimated as $q_{\text{con}} = \pi[(T_0 + 3\Delta T/2) - T_0]kD^2/2L$. This radiation and heat conduction estimation is for the steady state of the wire with a uniform

heat generation inside. Although it could not represent the experimental case precisely, it provides a sound first-order approximation of the radiation effect. The ratio of radiation to conduction is estimated as

$$\dot{q}_{\text{rad}}/\dot{q}_{\text{con}} \approx \frac{8\sigma T_0^3 L^2}{3kD}. \quad (14)$$

Taking Pt wire of data 1 as an example to evaluate the radiation effect since the average temperature increase ΔT (15.7 K) is much less than the ambient temperature (300 K), the radiation to conduction ratio is calculated to be 0.028 with Pt's thermal conductivity k as $71.6 \text{ W m}^{-1} \text{ K}^{-1}$.¹³ Since the ratio is much less than 1, it can be seen that the radiation heat transfer has less effects on the solution we established in this work. Similarly, in the measurement of MWCNT bundles and carbon fiber, the temperature rise is in the same magnitude as the Pt wire and the sample's thermal conductivity is higher than that of the Pt wire. In conclusion, the radiation heat transfer in this model is negligible compared to the heat conduction along the sample.

IV. CONCLUSION

In this paper, a fast transient technique was developed to characterize the thermophysical properties of microscale wires/tubes. This technique also has the capability of measuring nanoscale wires/tubes. Two methods were developed for data analysis to obtain the thermal diffusivity of the sample. Employing this technique, we measured the thermal diffusivity of Pt wires. The measurement results agreed well with the reference value. Our uncertainty analysis showed that the experiment has an uncertainty less than 10%. The thermal diffusivity of MWCNT bundles was measured and the average values were 1.07×10^{-5} and $1.46 \times 10^{-5} \text{ m}^2 \text{ s}^{-1}$ for type 1 and type 2, respectively. The real thermal diffusivity of individual MWCNTs based on alignment analysis was estimated around $1.18 \times 10^{-4} \text{ m}^2 \text{ s}^{-1}$. The measured thermal diffusivity of carbon fibers is $9.9 \times 10^{-5} \text{ m}^2 \text{ s}^{-1}$ on the average.

ACKNOWLEDGMENTS

Support for this work from the start-up fund of Iowa State University is gratefully acknowledged. Help from Dr. Namas Chandra of UNL for coordinating the collaboration is very much appreciated. The authors are grateful to Biqing Sheng, Dr. Zhaoyan Zhang, Kejun Yi, and Dr. Yongfeng Lu at UNL for using their high-power nanosecond pulsed lasers.

¹L. Lu, W. Yi, and D. L. Zhang, *Rev. Sci. Instrum.* **72**, 2996 (2001).

²T. Y. Choi, D. Poulidakos, J. Tharian, and U. Sennhauser, *Nano Lett.* **6**, 1589 (2006).

³J. Hou, X. Wang, P. Vellecheruvu, J. Guo, C. Liu, and H. M. Cheng, *J. Appl. Phys.* **100**, 124314 (2006).

⁴P. Kim, L. Shi, A. Majumdar, and P. L. McEuen, *Phys. Rev. Lett.* **87**, 215502 (2001).

⁵L. Shi, Q. Hao, C. Yu, N. Mingo, X. Kong, and Z. L. Wang, *Appl. Phys. Lett.* **84**, 2638 (2004).

⁶J. Hou, X. Wang, and J. Guo, *J. Phys. D* **39**, 3362 (2006).

⁷J. Hou, X. Wang, C. Liu, and H. Cheng, *Appl. Phys. Lett.* **88**, 181910 (2006).

⁸J. Hou, X. Wang, and L. Zhang, *Appl. Phys. Lett.* **89**, 152504 (2006).

⁹J. Guo, X. Wang, and T. Wang, *J. Appl. Phys.* **101**, 063537 (2007).

- ¹⁰J. Guo, X. Wang, L. Zhang, and T. Wang, *Appl. Phys. A: Mater. Sci. Process.* **89**, 153 (2007).
- ¹¹T. Wang, X. Wang, J. Guo, Z. Luo, and K. Cen, *Appl. Phys. A: Mater. Sci. Process.* **87**, 599 (2007).
- ¹²J. V. Beck, K. D. Cole, A. Haji-Sheikh, and B. Litkouhi, *Heat Conduction Using Green's Functions* (Hemisphere, New York, 1992), p. 482.
- ¹³F. Incropera and D. Dewitt, *Fundamentals of Heat and Mass Transfer*, 5th ed. (Wiley, New York, 2002), Appendix A.
- ¹⁴R. Weast, *Handbook of Chemistry and Physics*, 64th ed. (CRC, Florida, 1983–1984), p. F-125.
- ¹⁵SPI Supplies (http://www.2spi.com/catalog/spec_prep/cured_silver_film.html).
- ¹⁶Electron Microscopy Sciences (<http://www.emsdiasum.com/microscopy/products/sem/colloidal.aspx>).
- ¹⁷F. Incropera and D. Dewitt, *Fundamentals of Heat and Mass Transfer*, 5th ed. (Wiley, New York, 2002), p. 133.